X. Solid Propellant Engineering

PROPULSION DIVISION

N67-29151

A. Pressure and Density Gradients in Propellant Gases, *O. K. Heiney*

The problem of determining the fraction of propellant energy required to accelerate propellant gases in the ballistic system of burning propellants utilized for acceleration of a piston has been studied intermittently since the time of La Grange.

The problem is of interest not only from an energy fraction standpoint, but also because its solution directly gives a value for the pressure profile in the gas and, therefore, a value for the pressure drop from static gas to gas at the base of the piston, moving at a velocity equal to that of the piston. The analysis is performed for essentially two cases, (1) when the velocity of sound in the combustion products is a function of the adiabatic flame temperature T_0; and (2) when the velocity of sound is a function of 7/10 of T_0, with the realistic results somewhere between these boundaries. The symbols used in this analysis are defined in Table 1.

1. Density Distribution Analysis

La Grange, as covered in Ref. 1, takes the continuity equation and applies it to the system illustrated in Fig. 1,

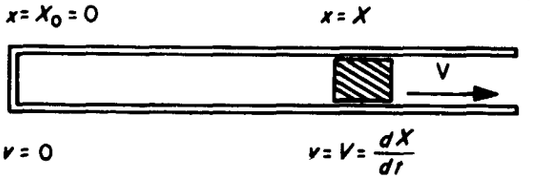

Fig. 1. System and boundary conditions

as follows:

$$\frac{\partial \rho}{\partial t} + \frac{\partial}{\partial x}(\rho v) = 0 \tag{1}$$

Then, La Grange assumes the constant density

$$\frac{\partial \rho}{\partial x} = 0$$

This assumption changes Eq. (1) to

$$\frac{1}{\rho}\frac{\partial \rho}{\partial t} = -\frac{\partial v}{\partial x} = C \tag{2}$$

Table 1. Definition of symbols

A	bore area
C_W	initial propellant charge
E_G	kinetic energy in accelerating gas
F_P	impetus of propellant
g	acceleration due to gravity
m_p	mass of propelled device
P_0	static pressure
P_s	pressure at base of shot
P_{av}	average plenum pressure
R	gas constant
T	gas temperature
T_0	isochoric flame temperature
V	piston velocity
v	gas velocity
V_c	plenum volume
X_0	initial piston reference
X	distance from piston base to X_0
x	chamber reference
γ	gas specific heat ratio
ρ	gas density
δ	density distribution factor

In turn, Eq. (2) is integrated with the boundary conditions shown in Fig. 1, giving

$$\int_0^v dv = C \int_0^x dx \qquad v = Cx \tag{3}$$

The boundary conditions also give

$$C = \frac{1}{X}\frac{dX}{dt}$$

then

$$v = \frac{x}{X}\frac{dX}{dt} \tag{4}$$

In Eq. (3), it is shown that the constant density assumption of La Grange will directly result in a linear gas velocity profile. Constant density is then a sufficient condition for velocity linearity, although not a necessary condition.

The energy in the gas using the above approach is then:

$$E_G = \frac{1}{2}\int_0^X A\rho v^2 dx = \frac{A\rho}{2} V^2 \int_0^X \frac{x^2}{X^2} dx$$

$$= \left(\frac{1}{2}\right)\left(\frac{1}{3}\right) A\rho X V^2$$

but

$$A\rho x = \frac{C_W}{g}$$

therefore

$$F_G = \left(\frac{1}{2}\right)\left(\frac{1}{3}\right)\frac{C_W V^2}{g} = \frac{1}{2}\frac{C_W V^2}{\delta g} \tag{5}$$

where

$\delta = 3$ for the La Grange solution.

The factor δ was introduced by Hirschfelder (Ref. 2) in his extension of the work of Kent (Ref. 3), who allowed the gas density to vary, and solved for δ as a function of the charge-to-projectile mass ratio.

Solutions of the form

$$\delta = f(C_W/m_p g)$$

are useful for the approximate closed-form ballistics of Hirschfelder, but are less useful for incremental computer solvable interior ballistic systems such as that discussed in a previous JPL report (SPS 37-44, Vol. IV, pp. 167–170). The results obtained by La Grange with $\delta = 3$ essentially state that the energy in the accelerating gas is equivalent to ⅓ of the gas mass traveling at the shot velocity. This is a good approximation at velocities where the gas density is almost constant. This approximation is inaccurate, however, at velocities where the density is no longer uniform.

For incremental computations, δ is most effectively formulated as a function of shot velocity. To accomplish this, however, it is first necessary to describe the density variation behind the projectile as a function of shot velocity. It is then assumed that a linear velocity gradient exists behind the shot and that isentropic flow relations may be used during an interval to describe the flow behind the shot. The flow, during the short interval

considered, must be considered as quasi-isentropic. According to Ref. 4, the density ratio then becomes:

$$\rho/\rho_0 = \left(1 + \frac{\gamma - 1}{2}\frac{v^2}{gRT}\right)^{-1/\gamma-1} \qquad (6)$$

The question then arises as to what temperature should be used to define the speed of sound in the environment of the burning gases. An upper bound for the temperature would be the isochoric flame temperature of the gases, T_0, while a reasonable lower bound would be 7/10 T_0. The analysis is then carried out for these two temperature extremes. For lower velocity ($< 3{,}000$ ft/sec) and during propellant burn, the values near T_0 are probably more accurate. At higher velocities, and subsequent to propellant burnout, the temperature tends to fall from the T_0 value. The results of Eq. (6) are illustrated in Fig. 2 for $\gamma = 1.222$ and $R\ T_0 = 375{,}000$ ft-lb/lb.

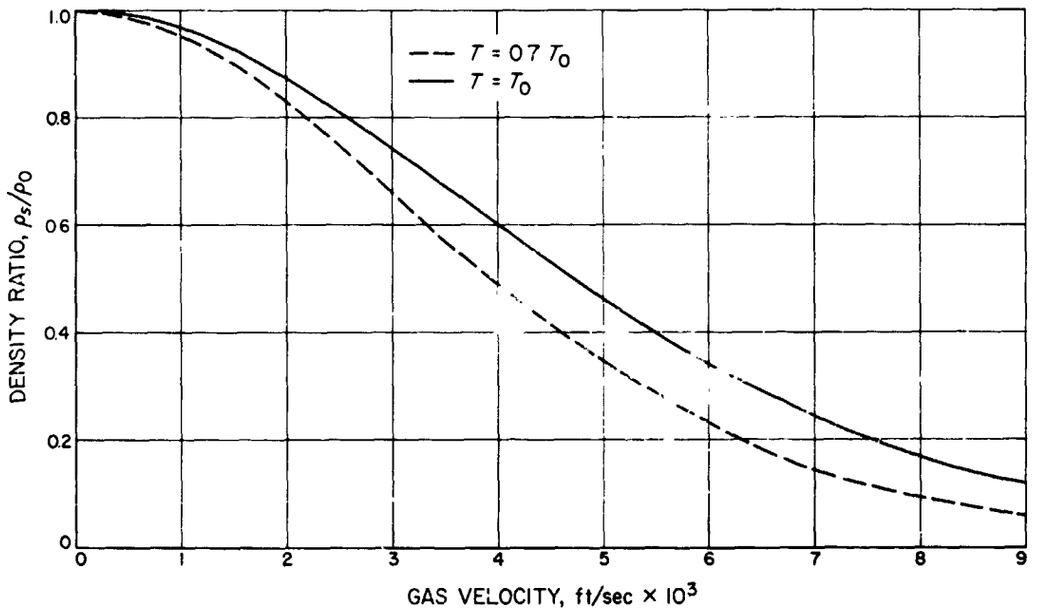

Fig. 2. Density ratio as a function of shot velocity

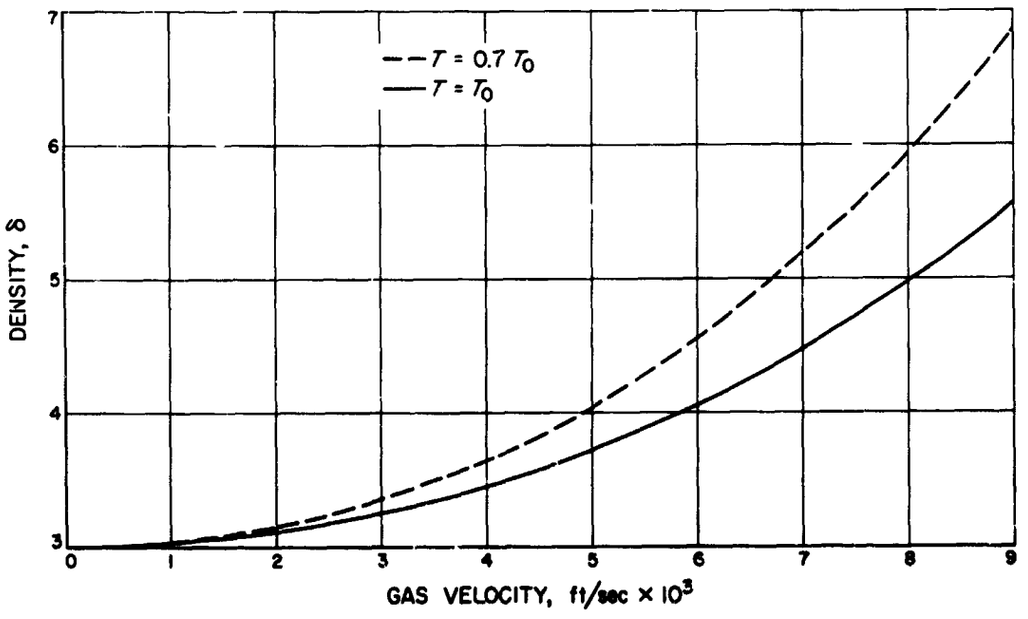

Fig. 3. Value of δ as a function of shot velocity

The energy increment in a small control volume of gas will then be

$$E_i = \frac{1}{2}\rho_N v_N^2 A \Delta x_N$$

and

$$E_G = \frac{A\rho_0}{2}\sum_N \frac{\rho_N}{\rho_0} v_N^2 \Delta x_N = \frac{1}{2}\frac{C_H}{g\delta} V^2 \qquad (7)$$

The value of δ is determined by performing the numerical summation of Eq. (7) on a digital computer. Fig. 3 illustrates the results of this procedure. As anticipated, the value of δ approaches 3.0 at low velocities.

2. Pressure Gradient Analysis

The determination of the pressure drop from P_0 or P_{ar} to the value at the base of the projectile, P_s, is central to any interior ballistic solution because the motion of the projectile is a function of P_s while the system energy equations give a value for P_{ar}.

A value for the ratio of P_s/P_0 may be obtained by the quasi-isentropic assumption previously used for densities.

$$P/P_0 = \left(1 + \frac{\gamma - 1}{2}\frac{v^2}{gRT}\right)^{-\gamma/\gamma-1} \qquad (8)$$

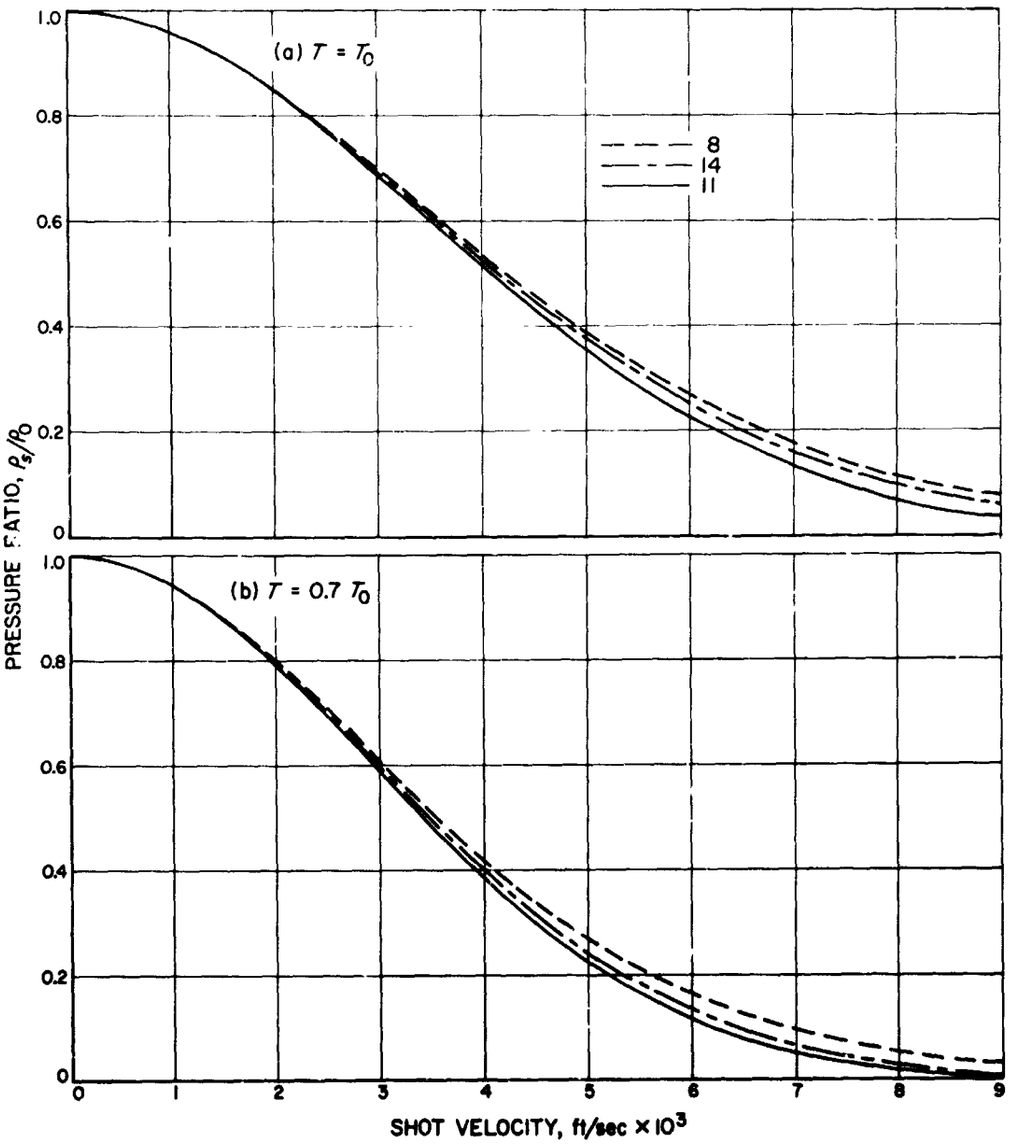

Fig. 4. Shot pressure to static pressure ratio as a function of shot velocity

The results of this relation are illustrated in Fig. 4 for the temperatures $T = T_0$ and $T = 0.7\ T_0$, respectively.

Another approach to the pressure gradient solution would be to assume a constant temperature process. In this case Eulers equation and the equation of state give

$$P = \rho RT \tag{9}$$

$$vdv = -\frac{dP}{\rho} \tag{10}$$

The combination of Eqs. (9) and (10) and integration give

$$\int_0^V vdv = -\int_{P_0}^{P_s} \frac{RT}{P}\, dP$$

$$\frac{V^2}{2} = -RT\, ln\,(P_s - P_0)$$

$$\frac{P_s}{P_0} = e^{-V^2/2RT} = e^{-V^2/2gF_P(T/T_0)} \tag{11}$$

The results of Eq. (11) are also shown in Fig. 4. The constant temperature equation always predicts a lower shot pressure than the quasi-isentropic relation. The required relation is that for P_s/P_{av}; Eqs. (8) and (11) give expressions for P_s/P_0. The problem being that for the interior ballistic formulism utilized, a term is already included for the energy in the accelerating gas, to give a value for P_{av}. A heuristically reasonable approach would be to assume that a relation of the form:

$$\frac{P_s}{P_{av}} = \left(1 + \frac{\gamma - 1}{2\phi}\,\frac{v^2}{gRT}\right)^{-\gamma/\gamma-1} \tag{12}$$

with

$$\phi > 1$$

would be satisfactory.

To investigate this possibility, a value must be developed for P_{av} which only accounts for the gas kinetic energy. This is accomplished as follows:

$$P_0 V_c - \frac{1}{2\delta}\, m V^2 = (\gamma - 1) V_c$$

$$1 - \frac{V^2}{2\delta\, gF_P(T/T_0)} = P_{av}/P_0 \tag{13}$$

The results of Section 1, giving $\delta = f(V)$, may then be employed with $\phi = 1.5$. The combined results of Eqs. (12) and (13) give a value for P_s/P_0 (Fig. 4). For the plotted values shown in Fig. 4 a ϕ of 1.5 was empirically chosen. This value of ϕ gives consistent results for both temperature extremes.

$$\frac{P_s}{P_0} = \frac{P_s}{P_{av}}\,\frac{P_{av}}{P_0} \tag{14}$$

3. Conclusion

The energy required to accelerate the combustion gases has a unique status in ballistic theory because, at low velocities, this energy may be considered second order and, at higher velocities, it assumes primacy. This energy is, in fact, the causal factor of the upper velocity limit of standard ballistic devices. The results expressed in Fig. 3 provide the δ values required for adequately averaging the gas acceleration energy in a given interior ballistic formulism, while the relations plotted in Fig. 4 give the bounds for determining the pressure gradient in a given device. Experimental ballistic firings will be conducted to empirically narrow these bounding relations. Recourse to empirical techniques is a requisite because the movement of a piston by burning propellant is neither adiabatic, isothermal, isentropic, or anything else.

B. Application Technology Satellite Motor Development, *R. G. Anderson, R. A. Grippi*

1. Historical Background

In January 1963 the Jet Propulsion Laboratory initiated a development program to provide a solid propellant apogee motor for a second-generation *Syncom* satellite. This program, under the management of the Goddard Space Flight Center, was designated *Advanced Syncom*. It was to result in a spin-stabilized, active repeater communications satellite weighing approximately 750 lb, operating at synchronous altitude (22,300 mi), which would handle voice communications, teletype, and monochrome and color television signals.

In January 1964 this program was redirected to include a number of experimental instruments in addition to the original communication instruments. This expanded program, the Application Technology Satellite (ATS), will result in a general-purpose satellite capable of operation at synchronous altitude with experimental instruments in meteorology, communications, radiation, navigation, gravity gradient stabilization, and various engineering experiments. To place these satellites in synchronous orbit, JPL will provide a solid propellant rocket motor

for the final required velocity increment at the apogee of the elliptical transfe. orbit. This rocket motor is designated the JPL SR-28-1 (steel chamber) or JPL SR-28-3 titanium chamber. At present, only the JPL SR-28-3 unit will be for flight use.

Previous progress reports on the development of this motor were published in SPS 37-34 to 37-43, Vol. IV.

2. Program Status Summary

The motor development program calls for static firing of 4 heavywall motors and 26 flightweight motors, including two with flight-design titanium chambers, prior to conducting an 8-motor qualification program. To date, 4 heavywall motors plus 24 flightweight motors have been static-fired, 4 of which were under simulated high-altitude conditions at Arnold Engineering Development Center (AEDC), Tullahoma, Tennessee. All of the flightweight motors tested to date were with Type 410 chromium steel chambers, with the exception of Dev. G-8T, G-9T, E-3T, and Q-9T, which used titanium chambers. During the past reporting period, two additional development units were tested. The testing of the first storage unit (Dev. F-1) was performed, after 16 months of storage, in January 1967. On March 10, 1967 a live unit (Dev. Q-9T) was tested as the fourth and final test in a program to evaluate an omnidirectional antenna design.

The ATS apogee motor qualification phase was conducted at AEDC in July and August of 1966. The results are reported in a previous JPL report (SPS 37-41, Vol. IV, pp. 91–96).

The first of five Applications Technology Satellites (ATS-B) was successfully launched in December 1966. The satellite is presently on station and functioning as planned.

3. ATS Storage Units

The three ATS apogee motors, cast in September 1965, have been stored at 80°F or ambient temperature following completion of post-loading requirements in November 1965. The units were processed and loaded to flight-standard procedures. All hardware components are of flight design with the exception of the chamber and the number of layers of chamber insulation. In place of the 6AL-4V titanium chamber, a Type 410 chromium steel unit was used since the titanium chambers were not available at the time the motors were loaded. The insulation configuration lacks one layer of 0.030-in. material at each end of the motor chamber. This difference in insulation configuration is a result of changes initiated in the flight design after the first titanium motor was fired in November 1965. These deviations from the flight configuration should not affect the storability of the motor.

These units are being removed at periodic intervals and subjected to various inspections. These inspections include weight determinations, visual examination of all components, dimensional checks, and hardware alignment. The last periodic inspection of the storage units was performed during November 1966 (SPS 37-43, Vol. IV).

The first storage unit (Dev. F-1) was statically tested at the JPL-ETS facility on January 31, 1967, approximately 16 months after being cast. Prior to static firing, the unit was subjected to a series of environmental tests including booster vibration, booster acceleration, and temperature cycle. These environments simulate, but do not duplicate, the conditions an apogee unit will encounter during the boost phase into orbit. Visual and radiographic inspection of the unit tested revealed no anomalies. Table 2 summarizes the weight and measurement data for Dev. F-1. This table includes data taken after the unit was cast in September 1965, and data recorded 16 months later just prior to static testing. All pre-fire data indicated that the apogee unit could be stored for at

Table 2. Weight and measurement data summary for ATS storage unit Dev. F-1

Parameter	Post-loading (Sept. 1965)	Prefire (Jan. 1967)
Chamber assembly weight, lb (chamber, insulation, propellant, and handling ring)	868.3	868.7
Nozzle assembly weight, lb	39.01	38.89
Hardware thrust alignment, in./in.	0.00007	0.00014
Propellant alignment		
Port diameter, TIR, in.		
Inches from nozzle boss		
4	0.015	0.015
14	0.017	0.016
24	0.014	0.011
Port diameter, in.		
Inches from nozzle boss		
4	10.147	10.191
14	10.143	10.168
24	10.139	10.140

least 16 months, after which it could survive a series of simulated launch environments.

The igniters for the storage units were originally assembled in February 1965. Prior to the static test of F-1, an igniter was disassembled and inspected. This visual inspection showed that the igniter hardware was not affected by long-term ambient storage.

Dev. F-1 was tested on January 31, 1967, at a grain temperature of 10°F while mounted in the vertical spin stand operating at 100 rpm. The unit appeared to operate normally during its 45-sec burning time. A post-fire inspection of the spent motor hardware indicated nominal operations. The data presented in Table 3 represent some of the motor's performance parameters and other pertinent data related to this unit.

Table 3. Static test data summary for ATS storage unit Dev. F-1

Test conditions	
Type of test	atmosphere/spin
Test location	JPL-ETS, Bldg. E-60
Date	Jan. 31, 1967
Run No.	E-731
Grain temperature, °F	10
Propellant weight, lb	764.7
Physical hardware (S/N)	
Chamber	P-32
Nozzle	F-26
Igniter	SYC-257
Squib	SDI-56
Pressure data	
Characteristic velocity, W*, ft/sec	4903.2
Chamber pressure integral, psia-sec	8857.7
Igniter peak pressure, psia at msec	*
Chamber ignition peak pressure, psia at msec	229 at 30
Chamber starting pressure, psia at sec	103 at 0.19
Chamber run peak pressure, psia at sec	243 at 34
Time	
Ignition delay, msec	10
Run time, sec	44.96
Nozzle dimensions	
Throat diameter, in.	
initial	4.083
final	4.106
average	4.095
Throat erosion (area), %	1.13

*Amplifier malfunction, data not available.

A complete analysis of all data related to this first storage unit appeared nominal with the exception of the characteristic velocity value (W^*). The measured value of W^* was 4903 ft/sec, approximately 1% below the average values obtained during testing of the development and qualification units. All data measurements related to W^* have been checked several times and appear accurate. A review of past ATS motor firings indicates that some decrease in motor performance may occur after the unit has been stored for 10 to 12 mo. A detailed review of all data related to this storage problem is being conducted and will be reported in a future SPS.

4. ATS Omnidirectional Antenna Test No. 2

The second omnidirectional antenna test was conducted at the L-ETS facility on February 17, 1967. These antenna tests are conducted jointly by JPL and Hughes Aircraft.

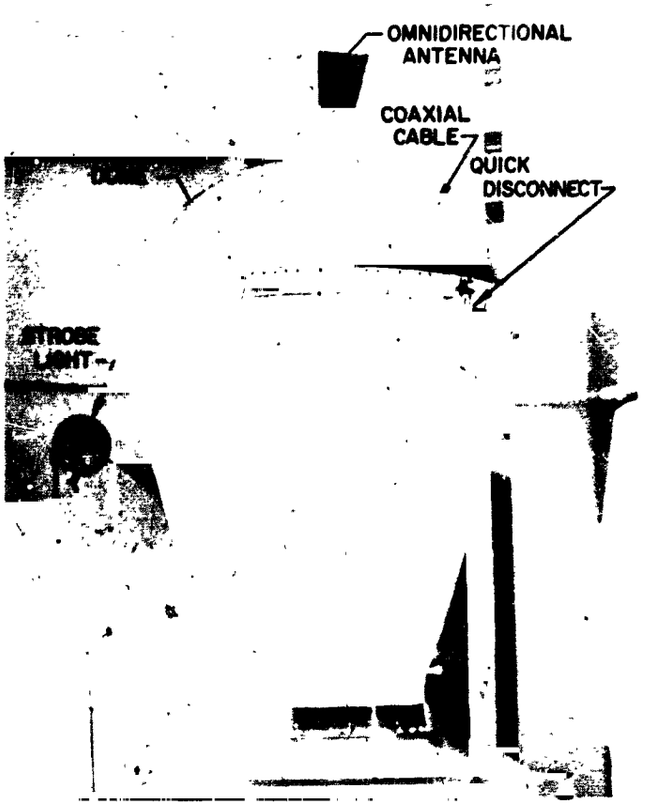

Fig. 5. Omnidirectional antenna-dome combination on apogee motor

The antenna for Test No. 2 was structurally modified based on the results of Test No. 1 (SPS 37-43, Vol. IV). The major design changes were an increase in the thickness of the fiberglass dome and in the method of attaching the antenna to the hemispherical dome. In the present configuration, the antenna is attached to a fiberglass cone which, in turn, is bonded to the main spherical dome.

The purpose of this test was to evaluate the release mechanism of the redesigned antenna-dome combination. The test consisted of releasing the antenna coaxial cable disconnects and confirmation of the antenna's free-flight path. These design changes were evaluated to ensure the structural integrity of the unit during its release and free-flight period. Fig. 5 shows the antenna-dome combination.

Since the first test confirmed that the ignition impulse was sufficient to release the antenna, the same apogee motor configuration was used for Test No. 2. During this test, the following JPL motor hardware was used:

(1) Motor Chamber P-6 (inert grain).

(2) Nozzle F-18.

(3) Igniter Basket, SYC-284.

(4) Squib, PC-37, S/N 37897.

The test setup consisted of the equipment shown in Fig. 6. The motor was mounted on the vertical spin test stand at the north test bay of Building E-60, at the JPL Edwards Test Station. Throughout the test, the motor and test article were spun at 100 rpm. Four 16 mm

Fig. . Pre-test installation of test article and high-speed cameras

Fastex cameras, operating at 2,000 frames/sec, were used to photograph the release and initial free flight of the antenna-dome combination. A 16 mm Milliken camera, operating at 500 frames/sec, was used for overall test coverage. Chamber pressure was recorded by two pressure transducers while another transducer recorded igniter basket pressure. The output of all transducers was recorded on an oscillograph (paper speed of 40 in./sec). A special circuit was created to indicate the release of the coaxial cables. The signal indication, which occurs after the antenna has traveled 0.25 in., was also recorded on the oscillograph.

The Fastex camera does not have the capability of incorporating a timing mark on the film; therefore, a strobe light was placed within the range of sight of all Fastex cameras. The strobe light was triggered at the same time current was supplied to the squib, thus producing on the film a positive indication of ignition sequence start. Fig. 7 shows the electrical circuits for the high-speed cameras, igniter ignition, and strobe light. As shown in the figure, the firing of the squib and strobe light and the starting of each camera were controlled by a Fastex goose box. The test was initiated by actuating the start switch on each goose box.

Following a dry run, during which the five cameras were tested, the test was performed. All data were adequately recorded, except for ignition current. The oscillograph revealed that it was still possible to correlate the start of the ignition sequence without an ignition current trace. At the time current was supplied to the squib circuit, a slight noise signal was generated in all pressure transducer circuits. This noise signal is discernible on all transducer traces recorded on the oscillograph (Figs. 8 and 9). This noise signal corresponds to zero time (t_0) or the first indication of squib current.

The results of the recorded pressures (Test No. 2) are given in Fig. 8. A comparison of the oscillograph records from Test No. 2 with those of Test No. 1 (Fig. 9) shows excellent agreement in both pressure levels and times.

The impulse from the igniter resulted in a nominal release of the antenna-dome combination with visual estimates giving a straight-up free-flight height of approximately 150 ft. The antenna was structurally intact throughout the trajectory, except for one coaxial cable which separated from the dome during its flight. Upon impact, the dome hit the ground at the antenna position, causing the fiberglass cone to separate from the dome,

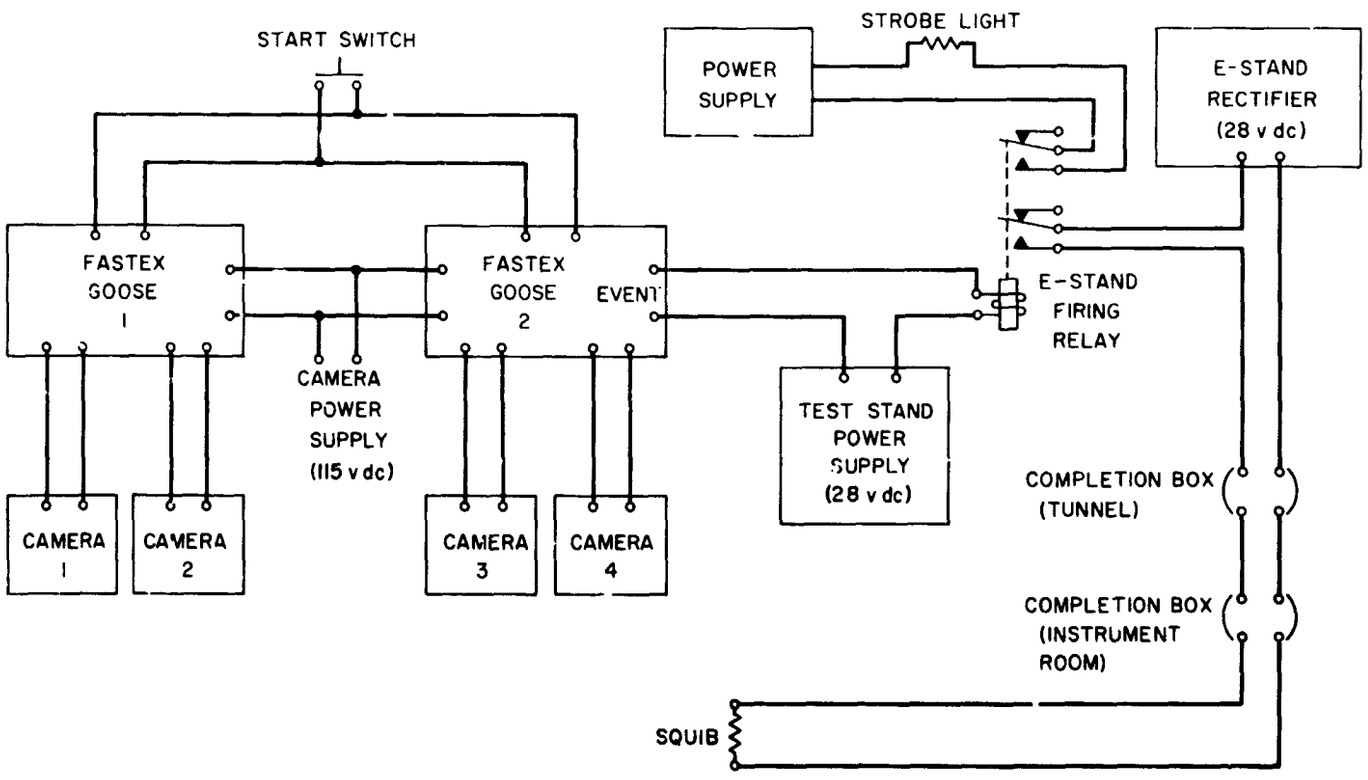

Fig. 7. Electrical diagram of high-speed camera and igniter ignition circuit

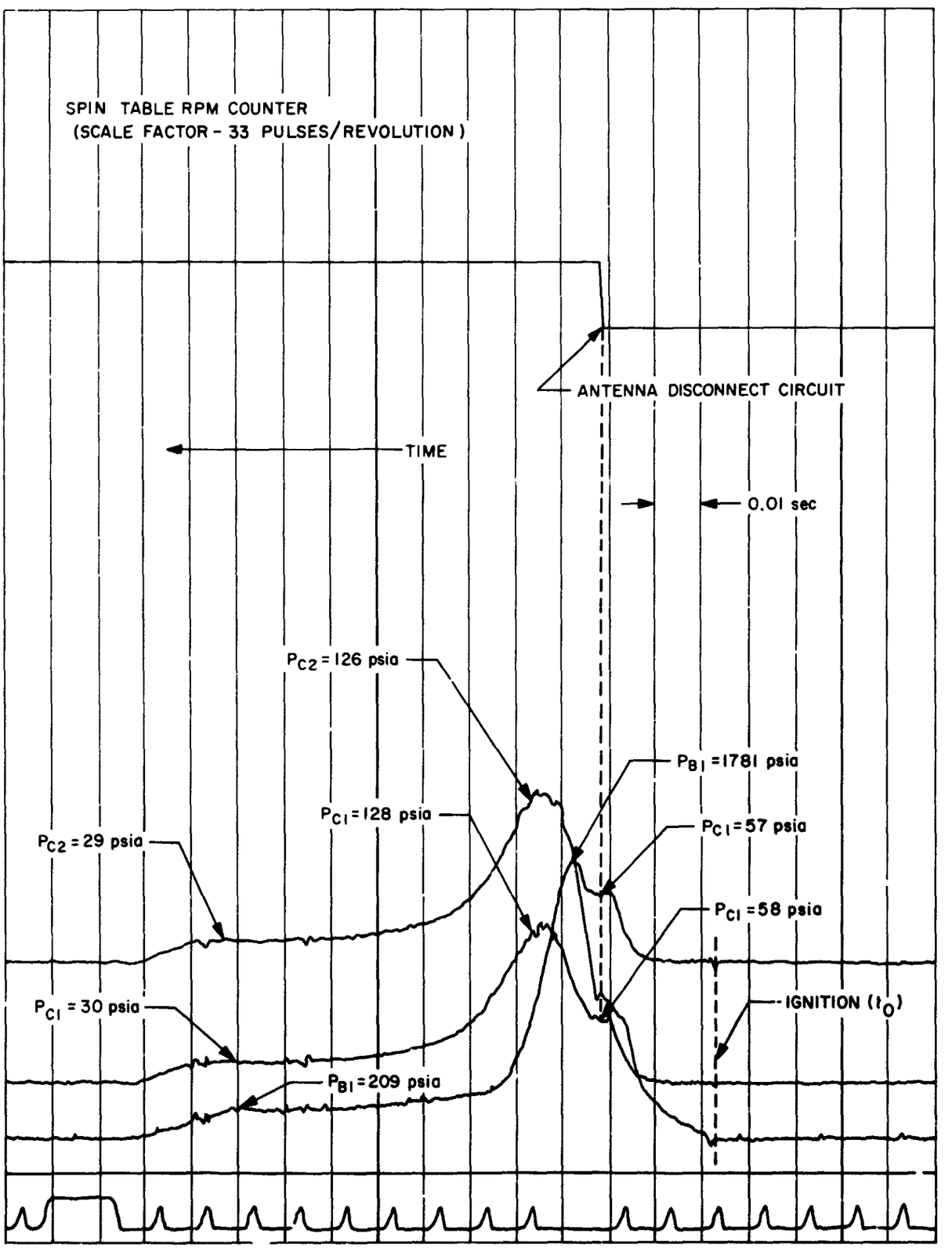

Fig. 8. Motor ignition characteristics—omnidirectional antenna Test No. 2

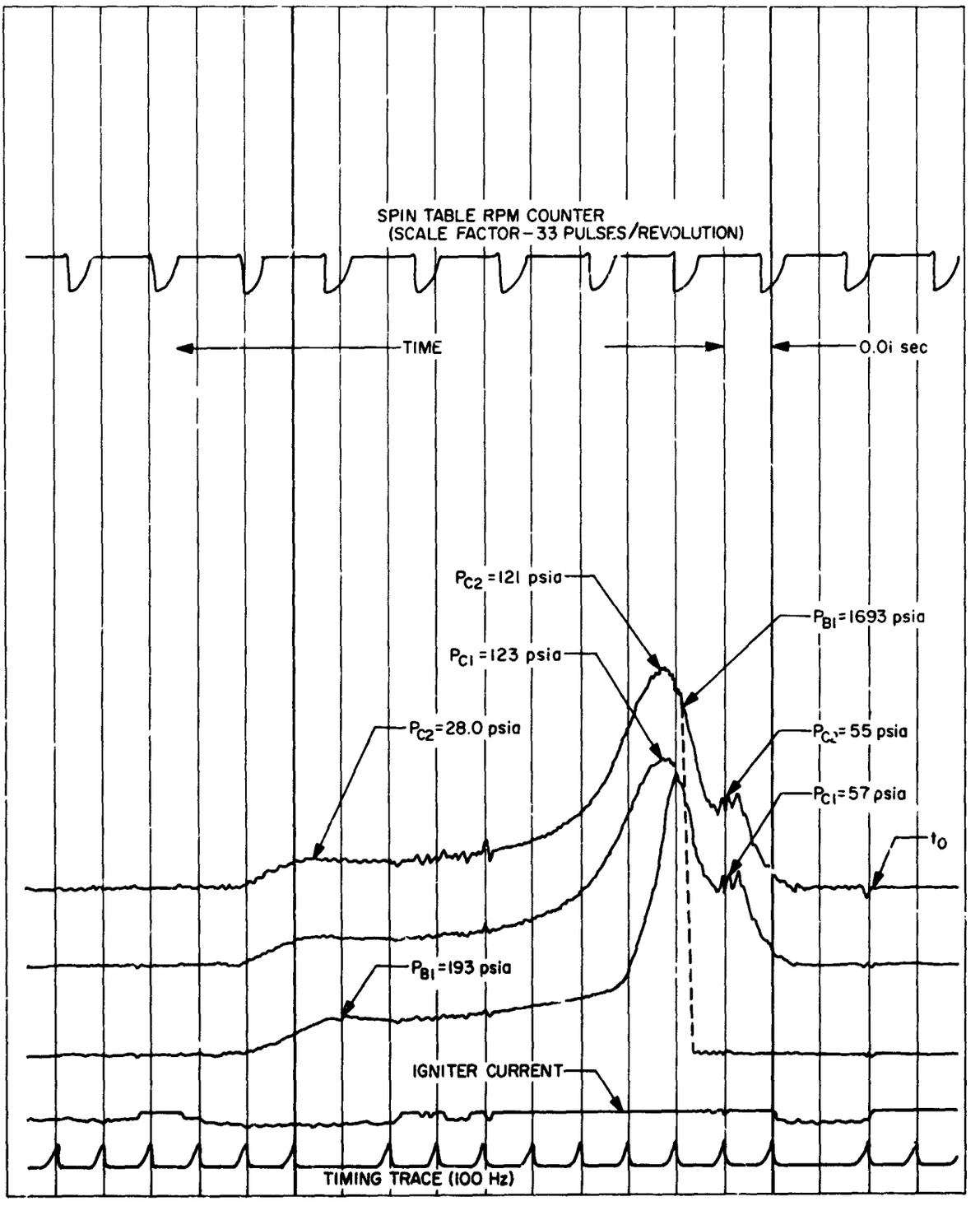

Fig. 9. Motor ignition characteristics—omnidirectional antenna Test No. 1

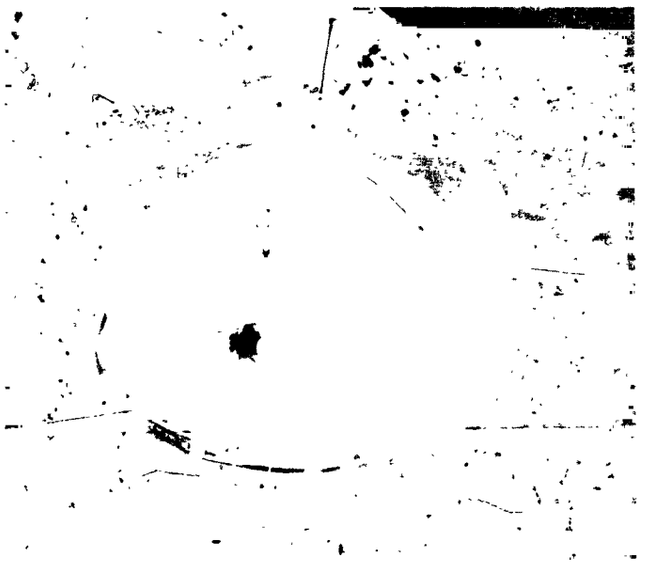

Fig. 10. Omnidirectional antenna-dome combination after test

and slightly damaging an antenna bracket. Fig. 10 shows the post-fire condition of the antenna at impact. The antenna disconnect circuit opened approximately 25 msec after the first application of squib current. At this time, the antenna had traveled approximately ¼ in. from its original position. At release, the motor chamber pressure was 58 psia, which closely corresponds to the nozzle diaphragm rupture pressure. The antenna is probably released from the motor within milliseconds after the nozzle diaphragm ruptures. Therefore, the antenna is never subjected to the peak chamber pressure generated during the motor's ignition phase.

In summary, the igniter impulse was sufficient to separate the redesigned antenna-dome combination from the motor without structural damage. As demonstrated by visual and photographic coverage, the antenna was released and maintained a free flight path along the motor's centerline well beyond the spacecraft's VHF antenna. The retention of the coaxial cable brackets was the only difficulty encountered during the test.

The third and fourth omnidirectional antenna tests were conducted on March 9 and 10, 1967. Test No. 3 only employed the ignition impulse to release the antenna. This test was almost identical to Tests Nos. 1 and 2. Test No. 4 employed a live motor (full duration) as a final confirmation of antenna design and release mechanism. The detailed result of Tests Nos. 3 and 4 will be reported in the next SPS. Initial results from the last two tests indicate that the antenna design and its release mechanism are reliable and no future antenna tests are anticipated.

C. Lockseal Adaptation to Syncom and Application Technology Satellite Rocket Motors, *W. L. Dowler*

1. Program Summary

This investigation was conducted to determine the weight increase of the *Syncom* and *Application Technology Satellite* (*ATS*) rocket motors if thrust vector control were provided. The Lockheed Propulsion Company's Lockseal thrust vector control system was the device used in the investigation. The study consisted of determining the weight of the components aft of the cylindrical shell for the rocket motors, both with and without Lockseal, and auxiliary hydraulic equipment. The adaptation of the motors to the Lockseal required the addition of several components as well as the thickening of the aft closure so that the closure could withstand the forces and torques required to actuate the nozzle through the desired angular deflections.

The results of the study indicated that the inert weight increases would be 19.03 lb for the *Syncom* motor and 28.69 lb for the *ATS* motor. These results show that the installation of the Lockseal (TVC) system on the *ATS* motor is more efficient, from a weight standpoint than on the *Syncom* motor. The estimated mass fraction for the *Syncom* motor changed from 0.85 without a thrust vector control system, to 0.67 with the Lockseal. The mass fraction of the *ATS* motor decreased from 0.90 to 0.87.

2. Adaptation of Lockseal to Syncom and ATS Rocket Motors

The designs of the *Syncom* motor, the *ATS* motor, and the Lockseal were reviewed. This preliminary evaluation showed that only motor components aft of the cylindrical section required modification. It was also determined that: (1) the location of the nozzle pivot point should be deep inside the chamber; (2) the Lockseal should be as near as possible to the pivot point, since the torque required to rotate the nozzle is proportional to the fourth power of the distance from the pivot point to the center of the Lockseal; (3) the Lockseal should be manufactured with specially prepared silicone rubbers capable of withstanding high pre-flight sterilization temperatures of 275°F. The selected silicone elastomer is designated Rubber Compound No. S-4 by Lockheed. This silicone elastomer also has a low shear modulus which minimizes the torque required to rotate the nozzle.

Table 4. Thrust vector control system parameters[a]

Parameters	Syncom	ATS
Nozzle deflection (2 axes), deg	±5	±5
Total number of operating cycles (each axis)	40.0	40.0
Actuator stroke, in.(±)	0.75	1.25
Actuator distance from center of rotation, in.	6.13	11.5
Maximum actuator force, lb	450.0	345.0
Nozzle moment of inertia,[b] lb in. sec^2	6.29	33.6
Actuator system pressure, lb/in.^{2}	1500.0	1500.0
Nozzle angular velocity, max., deg/sec	0.6	0.6
Distance between attachment points,[c] in.	6.75	9.25

[a]Note. In addition, the components of the servo-actuator system are designed to operate under adverse environmental conditions as follows (1) high vacuum of deep space, (2) temperature limits between −40 and +170°F after being subjected to six dry heat sterilization cycles at 135°C for 60 hr each and six surface exposures to Freox gas at 50°C for 24 hr

[b]About center of rotation of nozzle.

[c]Ends to be equipped with rod end bearings

The thrust vector control requirements included in Table 4 and the motor physical and geometrical data were used to compute the Lockseal configurations; the resulting motor configurations designed from these data and calculations are shown in Fig. 11 and 12. Servo-actuators were designed to move the nozzles through the desired rotation angle. The installation of these servo-actuators, as presently designed, was responsible for the major modifications to rocket chamber components.

The Lockseal adaptation to the *Syncom* rocket engine is shown in Fig. 11 and the weight distribution among components before and after the Lockseal adaptation is listed in Table 5. Fig. 13 is a plot of the torque as a function of the nozzle deflection angle. The aft closure was equipped with two sets of ears 90° to each other on the knee of the aft closure to hold one end of the actuators. Originally, the closure was designed to withstand an internal pressure only slightly larger than the design chamber

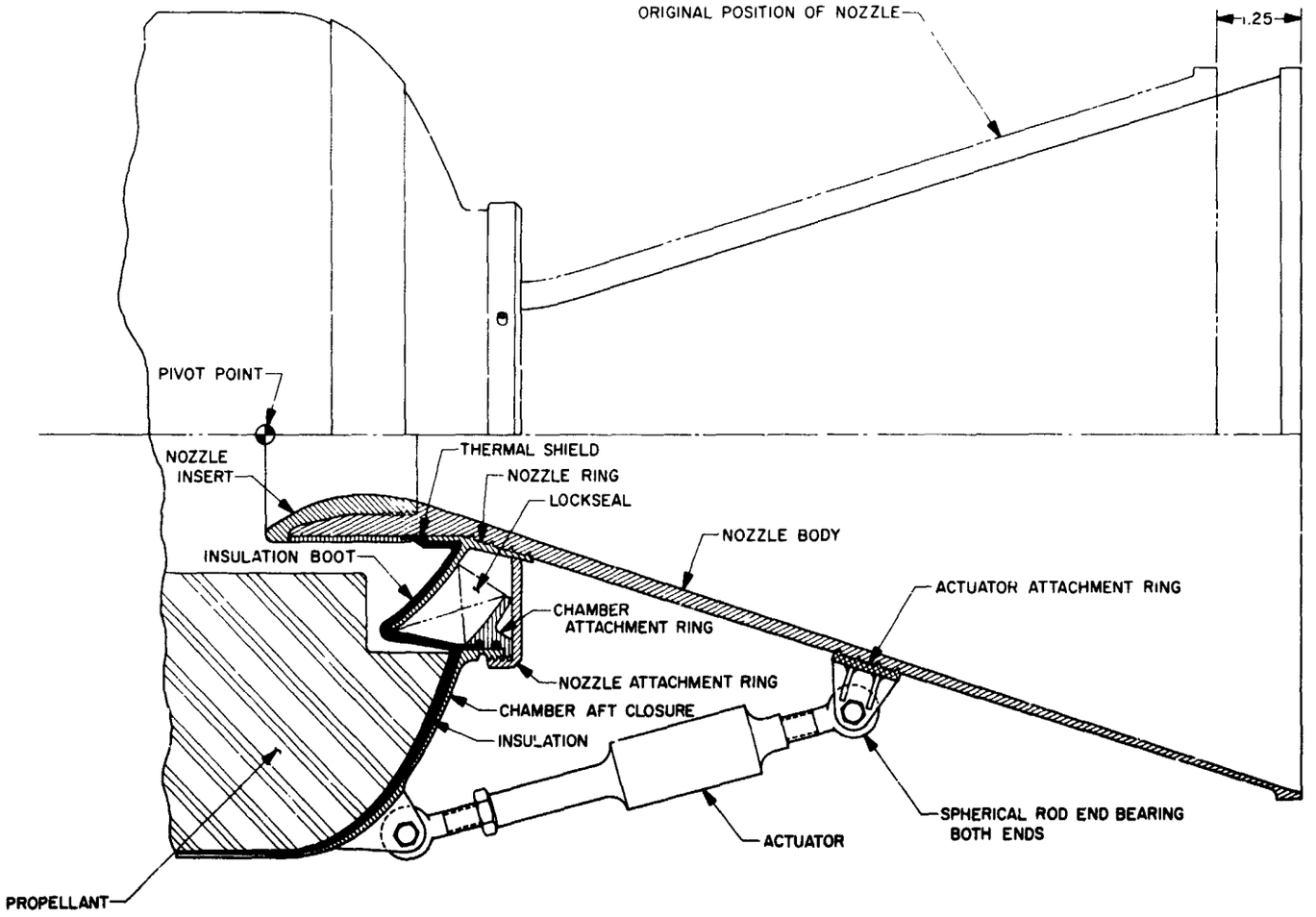

Fig. 11. Modification for adaptation of Lockseal thrust vector control system to *Syncom* rocket motor

pressure of the unit; this resulted in a thin and lightweight component. In the Lockseal adaptation, the shell must withstand the additional forces and torques of the actuators and Lockseal, and must, therefore, be made thicker. The required thickness was determined from a simplified model, consisting of a flat circular plate fixed around its edges and acted upon by a moment at the center. To minimize the weight of the aft closure, the combined stress produced by the moment and the internal pressure was made approximately 5% less than the yield strength of the material. This resulted in a wall thickness of 0.026 in., an increase of 0.012 in. at the thinnest section. With the greater wall thickness and the addition of ears, the increase in weight is approximately 0.50 lb.

The inside contour of the nozzle was not altered; however, the outside surface was modified to accept the aft end of the Lockseal and metal rings for seal and actuator mounting. The gas path is altered because of the Lockseal so that only the inside surface of the nozzle is exposed to the high temperature gases. This permits thinning of the nozzle wall with a consequent weight reduction of approximately 0.1 lb.

The Lockseal consists of two 6Al 4V titanium rings separated by a series of aluminum and silicone rubber washers. The forward ring is bonded to the forward end of the nozzle body with epoxy cement. The aft nozzle ring is machined with a flange which is retained in position against the chamber aft boss by a nut. A peripheral

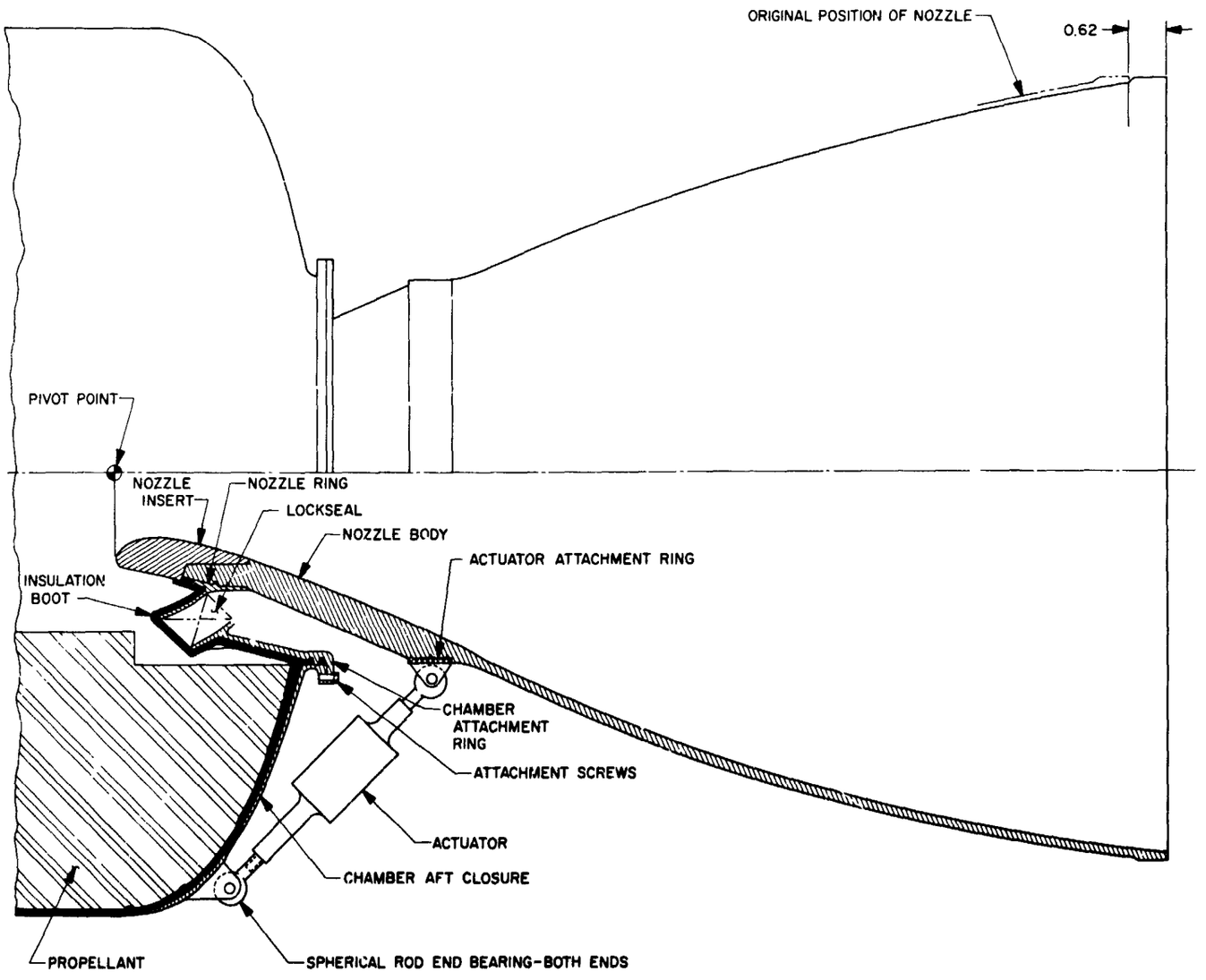

Fig. 12. Modification for adaptation of Lockseal thrust vector control system to ATS rocket motor

Table 5. *Syncom* motor weight

Motor weights	Original design, lb	Lockseal design, lb
Propellant	60.39	59.24
Total motor assembly	70.86	88.74
Weight changes		
Nozzle insert	0.22	0.22
Nozzle body	2.47	2.37
Insulation boot	0.34	0.56
Chamber attachment ring	—	0.64
Nozzle attachment nut	—	0.39
Lockseal components	—	0.78
Actuator attachment ring (on nozzle)	—	0.64
Chamber aft closure	0.48	0.98
Nozzle ring	0.88	0.53
Servo actuator system[a]	—	16.31
Propellant weight change	—	(−1.15)
Total weight	4.39	22.27
Net difference	—	+17.88
Mass fraction	0.852	0.668

[a]Includes. N_2 container, squib valve, regulator, hydraulic reservoir, 2 actuators, checkout ports, burst diaphragms, hydraulic lines and fittings, hydraulic fluid, and collection reservoir.

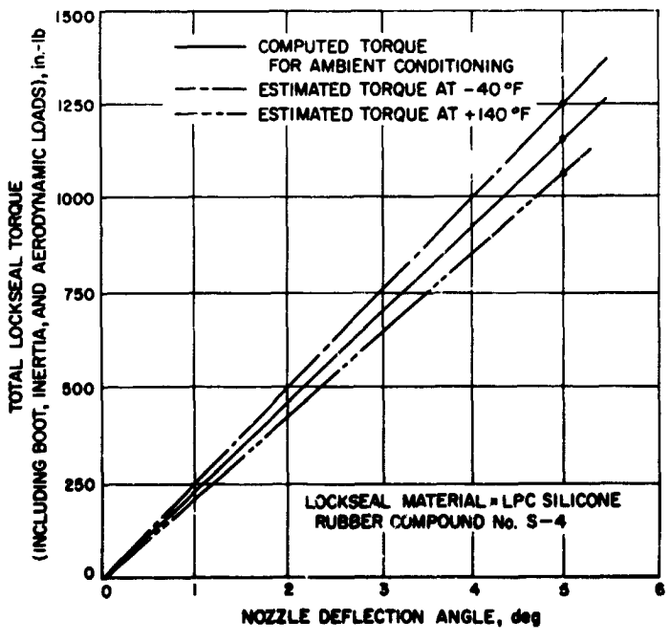

Fig. 13. Total Lockseal torque versus nozzle deflection angle for *Syncom* rocket motor design

O-ring in the aft ring prevents gas leakage between the chamber aft boss and the Lockseal ring.

The servo-actuator system consists of a pneumatic reservoir, a squib valve, a pneumatic regulator, a hydraulic reservoir, pitch and yaw actuators, and an oil return reservoir. This system is shown in Fig. 14, and values for the design parameters are included in Table 4. The estimated weight of the servo-actuator system for the *Syncom* motor was 16.31 lb.

A hydraulic system was selected to keep the overall weight to a minimum; however, electromechanical and pneumatic systems were considered. Electromechanical actuators were rejected because of the need for a larger power source. Pneumatic actuators were objectionable since these would result in soft systems because of the compressibility of the actuating fluid.

Additional components required to complete the thrust vector control system include a heat shield to protect the components of the Lockseal and various retaining pins securing the actuators to their respective attachment points. The thermal shield consists of an insulating boot which prevents the hot erosive gases of the rocket engine from impinging upon the components of the Lockseal. A thickness of 0.19 in. was estimated necessary to protect the Lockseal components during the rocket engine firing time of 45 sec. This insulation weighs approximately 0.55 lb as compared to the existing insulation which weighs 0.34 lb.

Retaining pins, acting in shear, will secure the two actuators to the chamber and the nozzle ears. The four pins which tie the spherical rod end bearings of the actuators to the ears weigh approximately 0.048 lb.

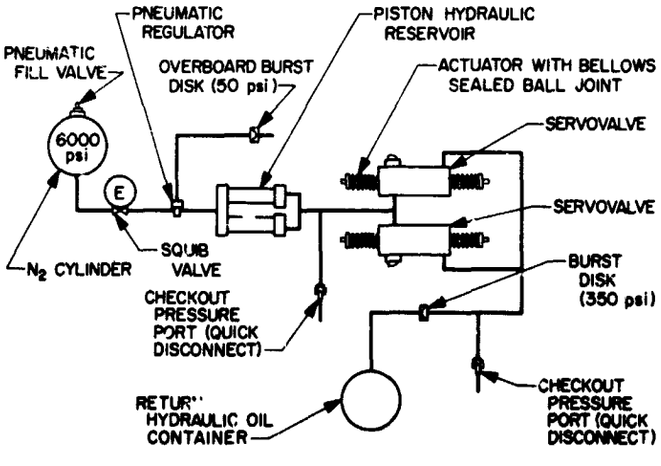

Fig. 14. Actuator system schematic

The weight of the bracketry required to fasten the auxiliary components of the servo-actuator system was not included in this weight analysis because much of it could possibly be provided by adjacent spacecraft structure. It is believed, however, that the weights of the servo-actuator components are conservative and will probably account for the greater part of the weight of the bracketry required if this is not the case.

It was necessary to remove an annular-shaped piece of propellant to allow the gimballed nozzle to pivot freely. The weight of the propellant removed is 1.15 lb.

The *ATS* motor required modifications similar to those of the *Syncom* motor. Several trial designs of the Lockseal for the *ATS* motor resulted in high torques. Therefore, it was necessary to install the Lockseal inside the chamber to achieve lower torque. This configuration, which required the insertion of a conically shaped spacer between the attachment boss on the aft closure and the Lockseal, is shown in Fig. 12. The weights of components in the Lockseal adaptation on the *ATS* motor are tabulated in Table 6. Fig. 15 indicates the torque required as a function of the nozzle deflection angle.

Table 6. *ATS* motor weight

Motor weights	Original design, lb	Lockseal design, lb
Propellant	760.0	751.63
Total motor assembly	840.7	861.02
Weight change		
Nozzle insert	2.33	2.33
Nozzle body	38.87	33.79
Nozzle ring	2.61	2.04
Chamber aft closure	4.83	6.29
Chamber attachment ring	—	6.84
Insulation	—	2.95
Lockseal	—	4.00
Screws and washers	0.29	0.29
Actuator attachment ring	—	0.94
Servo actuator system[a]	—	18.15
Propellant weight change	—	(−8.37)
Total weights	46.93	69.25
Net difference	—	+20.32
Mass fraction	0.904	0.873

[a]Includes: N_2 container, squib valve, regulator, hydraulic reservoir, 2 actuators, checkout ports, burst diaphragms, hydraulic lines and fittings, hydraulic fluid, and collection reservoir.

The nozzle weight is reduced by 3 lb because it is exposed to hot gas on one surface only. The ring connecting the Lockseal to the nozzle is slightly lighter than the original design; however, this weight is offset by the weight of the additional conical ring which joins the Lockseal to the chamber aft closure. The 6Al 4V titanium attachment ring weighs approximately 6.85 lb. The chamber aft seal is effected, as in the *Syncom* motor, by an O-ring between the attachment ring and the inside surface of the aft closure boss. The Lockseal is attached to the aft chamber by 36 screws in the flange, as in the original design.

The actuators are mounted between the aft closure and nozzle as in the *Syncom* motor. The aft closure must be thickened from 0.033 in. to 0.053 in. to withstand the additional forces developed by the actuator and the Lockseal. This thickness was estimated by considering the aft closure as a flat plate with fixed edges and acted upon by a moment at the center. The increase in thickness results in a weight increase of from 4.83 to 6.29 lb. The weight computed from this model results in conservative values for the thickness and, therefore, for the weight of the component.

3. Conclusions

The *Syncom* and *ATS* rocket motor designs can be modified to accept a Lockseal thrust vector control system.

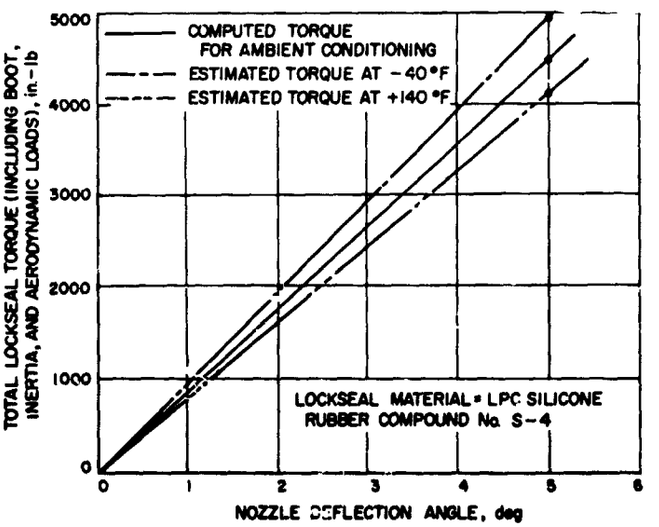

Fig. 15. Total Lockseal torque versus nozzle deflection angle for *ATS* rocket motor design

The weight of the servo-actuator system, which is essentially constant, causes the major increase in the motor inert weight. This results in a significant decrease in the mass fraction for the *Syncom* motor.

To install the Lockseal, the propellant charge must be reduced to provide clearance for the movable components. The *Syncom* and the *ATS* rocket nozzles had to be moved rearward by 1.25 in. and 0.62 in. respectively so as to minimize the increase in weight. This rearward shift changes the center of gravity and the moment of inertia of the rocket engines. Existing hardware, except the aft end, may be used with this thrust vector control adaptation for both units. The aft ends, however, require replacement with items having thicker walls to withstand increased forces and torques.

References

1. Corner, J., *Theory of the Interior Ballistics of Guns.* John Wiley & Sons, Inc., New York, 1950.
2. Hirschfelder, J. O., Kerschner, R. B., and Curtis, C. F., *Interior Ballistics,* NDRC Report A-142, Feb. 5, 1943.
3. Kent, R. H., "Some Special Solutions for the Motion of the Powder Gas," *Physics,* Vol. 7, 1936.
4. *"Equations, Tables, and Charts for Compressible Flow,"* NACA Report 1135, 1953.